

Local Universal Explainer (LUX) – a rule-based explainer with factual, counterfactual and visual explanations

Szymon Bobek szymon.bobek@uj.edu.pl¹ and Grzegorz J. Nalepa grzegorz.j.nalepa@uj.edu.pl¹

¹Faculty of Physics, Astronomy and Applied Computer Science, Institute of Applied Computer Science, and Jagiellonian Human-Centered AI Lab, and Mark Kac Center for Complex Systems Research

February 12, 2024

Abstract

Explainable artificial intelligence (XAI) is one of the most intensively developed area of AI in recent years. It is also one of the most fragmented with multiple methods that focus on different aspects of explanations. This makes difficult to obtain the full spectrum of explanation at once in a compact and consistent way. To address this issue, we present Local Universal Explainer (LUX), which is a rule-based explainer that can generate factual, counterfactual and visual explanations. It is based on a modified version of decision tree algorithms that allows for oblique splits and integration with feature importance XAI methods such as SHAP or LIME. It does not use data generation in opposite to other algorithms, but is focused on selecting local concepts in a form of high-density clusters of real data that have the highest impact on forming the decision boundary of the explained model. We tested our method on real and synthetic datasets and compared it with state-of-the-art rule-based explainers such as LORE, EXPLAN and Anchor. Our method outperforms the existing approaches in terms of simplicity, global fidelity, representativeness, and consistency.

1 Introduction

In recent years, a vast amount of research has been devoted to the development of explainable artificial intelligence (XAI) methods. Their goal is to bring trans-

parency and interpretability into the decision-making process governed by black-box machine learning models. This resulted in high expectations for applicability of XAI-based system to high-risk areas such as industry 4.0, medicine, financial markets, etc. These expectations were inflated not only by the rapid development of XAI algorithms, but also by legal regulations such as GDPR regulations [1], or the more recent AI ACT [2].

However, almost immediately the high hopes and expectations of making the ML/AI systems understandable for humans were cooled down when multiple empirical observations and expert-based critical reviews showed that the explanations very often cause more confusion than clarification. This has been noted by communities in almost each of the high-risk areas [3, 4, 5, 6] but also by the creators of XAI systems [7, 8].

There are several factors that contribute to the overall failure of the seamless adoption of XAI methods in certain areas. One of the most important reasons was that all of the XAI methods implicitly assumed some level of technical background in data science from the addressee of the explanations. This makes the interpretation of XAI results a non trivial task [8]. Furthermore, even rule-based explainers, which output is one of the most understandable by non-technical experts as reported in [9], tend to produce explanations which are be over-complicated.

Finally, all of the state-of-the-art methods focus only on one particular aspect of explainability, i.e. feature importance, rule-based explanation, counterfactual explanations, etc. Therefore, to obtain the full spectrum of explanations for a decision of a model, one has to combine the results of multiple different algorithms. However, they are usually based on different theoretical backgrounds and often use statistical learning to produce explanations, making them inconsistent (or sometimes contradictory) with each other. Additionally, all available local explainers use artificially generated samples to create explanations. This may cause the locality-fidelity paradox, as recently reported in [10], where local explanations incorrectly explain the behavior of a model, are overcomplicated and counterintuitive. Such a phenomenon arises from the fact that a large number of artificially generated samples in local neighborhood may still produce over-complicated decision boundaries or phantom explanations that rely solely on non-existing data samples and have no coverage in real-world data. It also causes the explanations to be unstable, as the randomness related to data generation may affect the way the explanation is created for the same instance in consecutive runs of the explanation mechanism. In this work, we address the aforementioned issues by proposing a model-agnostic method that generates simple, rule-based explanations that are local, counterfactual, and consistent with feature importance approaches such as LIME and SHAP. Furthermore, the method provides a way to assess the certainty of the generated explanation by providing a visualization of explanations over the

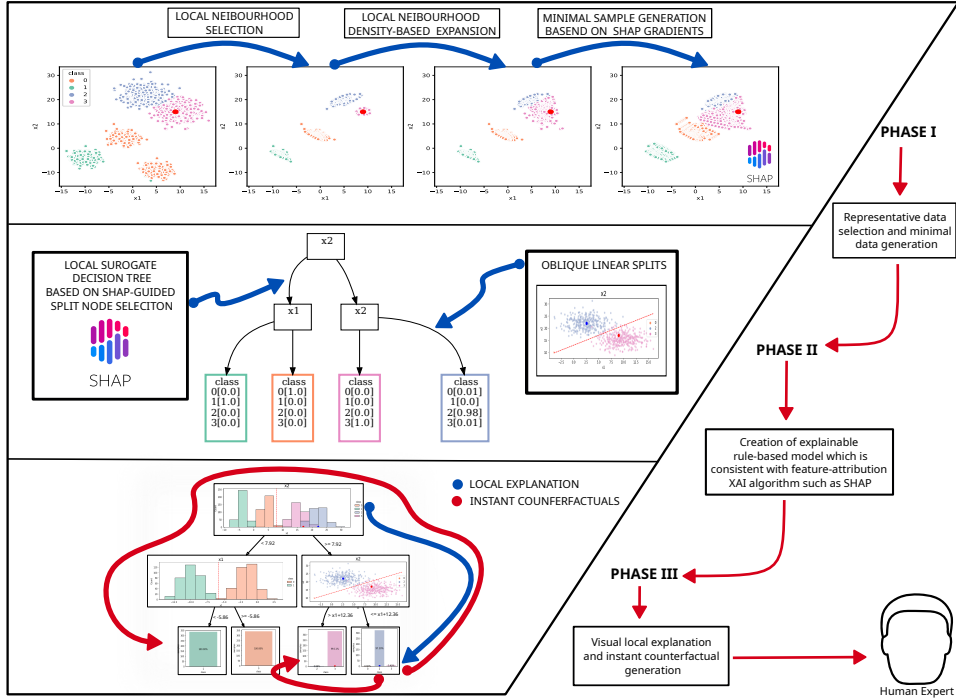


Figure 1: Diagram representing three phases of rule-based explainable model creation. The first phase is focused on selecting and refining representative dataset for local surrogate model creation. The second phase concentrates on generating an oblique, shap-consistent decision tree. The third phase provides visual presentation of local explanations as well as counterfactual generation mechanisms.

data distribution. The overview of the contribution of this paper is presented in Figure 1. The overall procedure is divided into three phases starting from data selection and preparation, through explainable local surrogate model training and visual presentation of explanations and counterfactuals.

As a backbone of our explanation mechanism, we used a decision tree structure. It allowed us not only to generate rule-based explanations, but also to immediately extract consistent counterfactuals by traversing the explanation tree in an appropriate way. We limited the use generated or perturbed data for training of the explanation model to avoid disrupting the distribution of the data and obtain the most plausible and representative counterfactuals. We compensated for the possible shortage in training instances by using SHAP importance values as a support in selecting features to construct explanation rules and generating samples only towards the direction of negative gradient of shap values which points

towards the direction of a decision boundary of a balckbox model. This allowed us to obtain explanations consistent with SHAP, which is one of the most popular methods used in the XAI field. Finally, we extended the possible tree nodes to contain simple oblique splits (based on linear inequalities rather than value-based inequalities), which we visualize on a 2D scatterplots. We show that our approach outperforms other state-of-the-art rule-based solutions with respect to global fidelity, representativeness, and simplicity and consistency with SHAP (or any other feature-importance attribution XAI technique used). We present the results obtained from a publicly available, fully reproducible benchmark. To the best of our knowledge, this is the first comprehensive comparison of local rule-based explainers available in the literature so far, not counting the work of G. Vilone, et. al [11, 12], which focuses on global rule-based explanations in contrast to our contribution.

The remainder of the paper is organized as follows. In Section 2 we describe the wide spectrum of existing XAI methods and place our work in that context. In Section 3 we provide a critical overview of rule-based explainers and form four requirements that every local, rule-based explainer should meet. We present our method in Section 4 followed by the evaluation given in Section 5. We summarize our work by providing its strong and weak sides in Section 6.

2 Related works

Explainable artificial intelligence aims to bring transparency, trust, and intelligibility to automated decision making systems based on artificial intelligence algorithms [13, 14]. Although such methods are currently experiencing a renaissance, the concept of explainability is not new and can be dated back to the times when expert systems were the most successful AI implementations [15]. However, due to the great successes of deep neural networks and other black-box ML algorithms, the topic of explanation and interpretability has been brought back to the main stream of AI research. One of the triggers for research in XAI in modern AI was the NASA XAI Challenge [16] and recent EU regulations, namely GDPR [17] and the AI Act [18], which moved the requirement of transparency of an AI system from the technical to the legal level.

However, there is no consensus among researchers on how this transparency is defined and, therefore, how it should be delivered. This results in multiple research paths on different types of XAI methods, which cover different aspects of explanations. In general, however, the primary goal of any explainable AI method is to provide some sort of insight that can be used by a human to understand how the model processes input data to the output. This insight can have a very differ-

ent form and can carry different amounts of information depending on the XAI algorithm used. It can also answer very different questions about the operational aspects of the AI model at very different levels of granularity.

From the perspective of granularity of explanation, one can classify the XAI algorithms into local explanations that focus on generating explanation around a particular instance and global explanations that aim at providing general explanation for a model as a whole. The most representative examples of the former are SHAP [19] or LIME [20], while the latter are mostly dominated by well established statistical methods such as partial dependence plots, accumulated local effects, functional decomposition, importance of permutation features or prototype discovery [21].

From the perspective of the robustness of the explanations, one can distinguish model-agnostic algorithms that do not depend on the model to which they can be applied and model-specific methods such as those which are designed to work with a particular type of the model. Model-agnostic methods treat the model they explain as a black-box, without any assumptions on its internal mechanisms. This makes them very robust solutions as they can be applied to any kind of system that converts a predefined set of inputs into the output. Examples of model-agnostic methods are algorithms already mentioned, such as SHAP or LIME, Anchor [22], LORE [23], EXPLAN [24] but also most global explainers [25]. However, model-specific methods leverage some of the properties of the algorithm they explain, which can boost their performance. In some cases, the model-agnostic method can be redesigned to be model-specific. The example of this is the SHAP method which has a model agnostic version in the form of KernelSHAP [26] and model-specific version such as TreeSHAP [27], or DeepSHAP [19] that are designed to work faster with different families of ML algorithms.

This classification can be further broken down into inherently interpretable models and post hoc explainers. The first group is formed by the AI systems that are interpretable by design, which allows one to explain its decision by tracking the process they were made. Linear regression and decision trees are the most commonly used methods among them. The trend of building efficient glass-box, inherently interpretable models instead of post-hot approaches is growing in popularity. This was first tackled in [28], where the author stated that there is no scientifically proven dependency between model complexity and its efficiency. A similar approach was presented in [29], where the authors present explainable boosting machines, a method that is interpretable and efficient. The post-hot model assumes that the explanation can be generated without any interference in the internal mechanics of the model that is being explained. However, the existence of post-hot and inherently interpretable models in one explanation mechanism is not mutually exclusive. In fact, a building block of many post-hoc explainers, such as model-

agnostic explainers mentioned before, are inherently interpretable models which locally mimic the behavior of the original model.

Finally, from the perspective of the form of the explanation one can distinguish three leading strategies of generating and presenting explanations: 1) feature importance attribution methods, 2) counterfactual and contrastive explanations, and 3) rule-based explanations. In the first group, the leading places are taken by algorithms such as SHAP, LIME or BreakDown [30]. Although they differ in the underlying mechanisms, they all provide local explanations in the form of feature importances and feature impacts. Such explanations can be used to answer the question of how different features affect the model decision for a particular instance. Although this form of explanation may seem to be one of the simplest, they are also one of the most popular ones. However, this simplicity is illusory and is prone to many serious interpretation errors, which was noticed in many recent works both from the data-science perspective [8, 7] as well as from the perspective of domain experts from different fields such as industry [4] or healthcare [3].

The group of counterfactual and contrastive explanations is formed by approaches such as [31]. The main goal of this type of explanation is to provide information on how to change the features of a given instance to change the classification result of the model. Among the most popular counterfactual explainers, there are: DiCE (Diverse Counterfactual Explanations) [32], which provides an explanation in the form of minimal perturbations needed to change the decision of a model for a particular instance; Actionable Recourse in Linear Classification [33], which provides a method of generating counterfactuals only perturbing the *actionable* variables that can be changed in reality. More methods can be offered by CARLA (Counterfactual And Recourse Library) [34] which is a framework that integrates multiple different methods for counterfactual explanations. All of the aforementioned methods focus solely on the counterfactual explanations, not providing any other means of insight into the model decisions.

Finally, rule-based explainers are dominated by three state-of-the-art algorithms, already mentioned: Anchor, LORE and EXPLAN. They provide explanations in a form of rules which are human-readable and can be interpreted easily even with non-data-scientists. The Anchor algorithm uses a modified beam search mechanism combined with a pure-exploration Multi-Armed-Bandit [35] to find rules that describe the class of an instance that is explained in its local neighborhood. It provides high-precision rules, which explain the decision of a black-box model for a particular instance; however, it does not provide counterfactual explanation at all. LORE and EXPLAN algorithms use a decision tree as the backbone of the rules-building mechanisms. This allows these methods to extract counterfactuals from the tree structure, not only the explanation of a current instance. However, they both use data-generation approaches that change the distribution of the orig-

inal data. This may result in the appearance of false counterfactuals in the form of phantom branches in a tree – branches that were created based solely on generated instances and have no coverage in the real dataset. Furthermore, they tend to generate rules which are overcomplicated and not consistent with SHAP values calculated for the explained instance, which is caused by the greedy nature of the decision tree mechanism. An interesting approach was presented in the RuleXAI [36] toolkit, where the authors used information on the relevance of features to filter attributes that should be used to form an explanation rule, which can improve consistency with methods based on the importance of features. However, the authors did not consider that the importance of the features used to generate a local explanation should be considered only in the locality of the instance being explained, otherwise it may cause serious misinterpretation of the results as reported in [8] and [30]. Furthermore, they used feature importance not corresponding to the type of the model they explain assuming that the important feature is utilized similarly by a non-parametric model like a decision tree and parametric one like neural network, or logistic regression, which is not true. Finally, none of the above methods provides visualization of the explanations that can help in the interpretation of the data.

In this work, we focus on post-host, model-agnostic, and local explainers. Motivation behind that arises from the target users of the explanation mechanism we aim at. Our goal was to design a method that will be addressed to non-data-scientist users, experts in the domain of interest, and that will solve the issues with existing rule-based explainers. For this purpose, we propose a method that is robust, model-independent, and highly human-readable and combines all forms of explanations into one consistent mechanism enhanced with visualization. The following section will state the problem formally and confront it with the state-of-the-art approaches.

3 Problem statement

In our work, we focus on explanations that can be used by non-technical user, particularly domain expert in a field. This limited our research to rule-based explainers, as their ability to be understood by experts is one of the highest [9], especially in the areas related to medicine, industry, and law where rule-based knowledge is used on a daily basis.

3.1 Critical overview of the existing rule-based explainers

In our work, we focus on local explanations, which are designed to explain a decision for a particular instance, as opposed to global explanations, whose objective

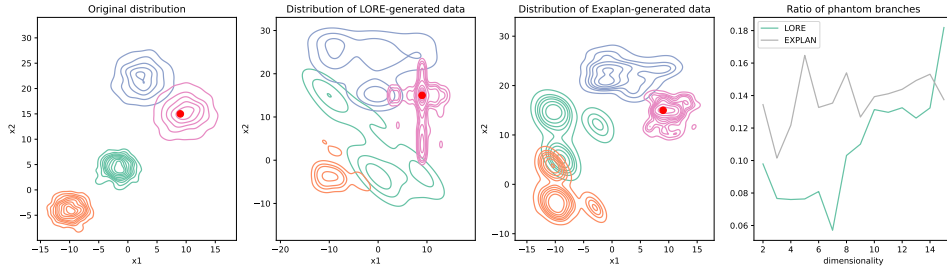


Figure 2: Impact of the generated data on the explanations generated with LORE and EXPLAN. The leftmost plot represents distribution of the original data, the following two plots show distribution changed by the data-generation algorithm used by LORE and EXPLAN. The rightmost plot shows how many phantom branches are generated from such an altered distribution. Such phantom branches may generate non-representative counterfactuals, like these marked in red circles.

is to explain an average behavior of the model on a given dataset. One of the basic criteria of the correctness of an explanation is its faithfulness. The explanation is considered faithful if $\Phi^{\bar{E} \rightarrow M(x_i)} = M(x_i)$, which means that the explanation provides the same prediction for an instance as the original model. Therefore, it is assumed that local extension is more faithful in the nearest neighborhood of the instance that is being explained than in the whole dataset, because it is assumed that the decision boundary at a subset of the data can be approximated by a simple model, such as a linear model in case of LIME or rule-based models in case of LORE, EXPLAN or ANCHOR. However, incorrectly selected neighborhood with many artificially generated samples may cause the production of an explanation model that is degenerated [10] causing the explanation to be unfaithful, counterintuitive and overcomplicated. Figure 2 presents the results of the experiment we conducted with EXPLAN and LORE to observe how the generation of artificial samples may affect the explanations. It can be seen that an altered distribution of the data causes the generation of multiple phantom branches that do not have coverage in the real data. In case of counterfactual explanation, this may result in building explanations that are not consistent with dataset and, hence, counterintuitive to the expert. It also makes the whole decision tree larger and more complex.

Moreover, the selection of the neighborhood for building local explanation cannot be simplified to just distance-based selection. The EXPLAN algorithm approaches this problem by including agglomerative clustering as a method of selecting representative samples. However, this is not always a correct strategy, as depicted in Figure 3. The figure shows that the neighborhood that is sufficient to locally explain the decision of the classifier can be limited to explaining the deci-

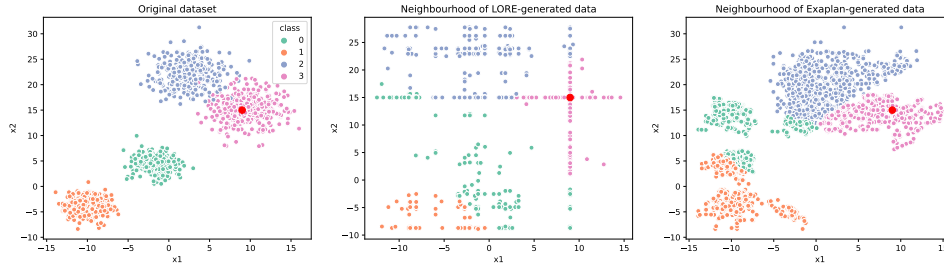


Figure 3: The differences in the local neighborhood defined by different rule-based explainers. The local neighborhood was generated for the instance marked red.

sion boundary between clusters 2 and 3. However, both LORE and EXPLAN will always include in the neighborhood other, possibly distant clusters of data, which do not necessarily should be considered as a local neighborhood.

Furthermore, all of the rule-based explanation mechanisms limit the presentation of the explanation to a form of textual rule. In most of the practical applications, such a textual representation might not be enough, especially when working with continuous values, where numerical thresholds set on rules' conditions are not always meaningful to the experts. The explanation has to be understandable to the user in order to be useful and to have practical value. Focusing only on one aspect of the quality of explanation can lead to degenerated results, as was shown in [37], where the authors represented a neural network as a decision tree with split conditions represented as linear algebra inequalities. Although the method achieved good results in terms of fidelity, from a practical perspective, it was yet another black-box model. Understandability is hard to measure; however, as reported in several empirical studies [38, 39, 9] the most understandable explanations are those that are visual, contrastive and rule-based. Despite that fact, none of the state-of-the-art rule-based explainer includes visual representation of explanation. Additionally, the rules are generated by decision tree algorithms, or rule-discovery algorithms that generate explanations in the form of conjunction of simple inequalities. This feature is motivated by the simplicity argument that states that the rule-based format of explanations is one of the most understandable [9]. However, in many cases, this is not true, especially when the approximated decision boundary is a linear function. In such a case, the rule-based approximation may overcomplicate it rather than simplify. The example of such a case was given in Figure 4 where the LORE, EXPLAN and Anchor decision boundaries were shown along with the original decision boundary of the model they explain.

Another aspect that is observable with state-of-the-art explanation mechanisms is the consistency and stability issues. The consistency can be analyzed from two

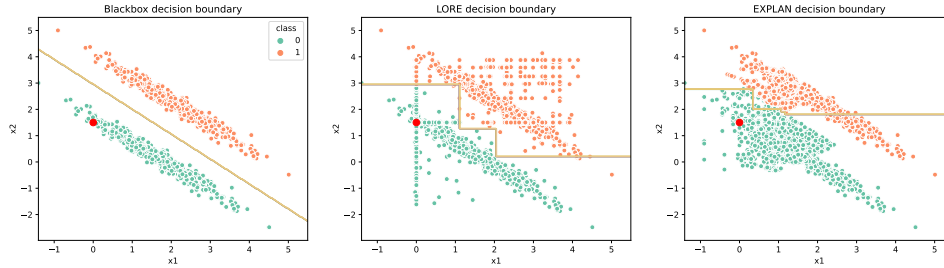


Figure 4: Decision boundaries of a blackbox model and local approximations of that boundary with LORE, EXPLAN and Anchor. It can be seen that in case of linear boundaries, that are hard to capture by tree-based inequalities the existing explainers produce overcomplicated and non-intuitive explanations.

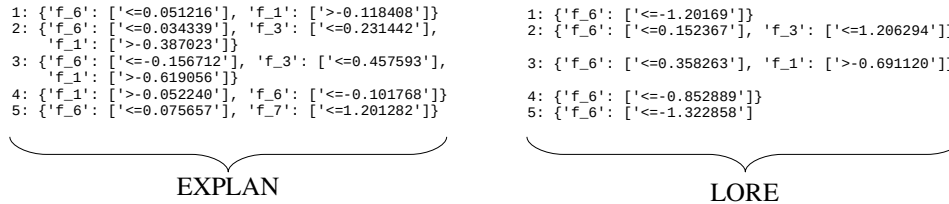


Figure 5: Five explanations generated for the same instance and the same dataset. It can be seen that the explanations are different in consecutive runs, making them less usable and less intuitive for users.

different perspectives: consistency of an explanation with respect to other types of explanations (e.g. consistency of factual explanation with feature-importance attribution explanation) and stability, which can be defined as consistency of the explanations generated by the explainer for the same instance (e.g. is the explanation for a given instance the same for consecutive calls of the explainer). From our experiments, we discovered that not only the state-of-the-art explainers are not consistent between each other, but due to the randomness of the data-generation technique they use, the explanations from the same explainer might be different for the same instance and the same initial dataset. This situation was illustrated in Figure 5.

In addition, the explainers focus mostly on one type of explanation: the factual one. Only LORE provides counterfactual explanations, while EXPLAN and Anchor do not. However, the counterfactual explanations of LORE suffer from the same problems as the factual explanation.

Finally, the available algorithms for rule-based explanations do not provide any means of extended quality assessment. Currently, the quality of the explanation is

measured in a similar way to the quality of a model predictions, with a variety of XAI-related metrics such as fidelity, stability, complexity, sensitivity, etc. [40]. However, such methods do not take into account the context of the explanation, such as the data distribution for which the explanation was generated, the uncertainty of the explanation model, and the uncertainty of the blackbox model. All of this information is vital to the quality assessment of the explanation.

In the following section, we define several requirements for the rule-based explanation to meet in order to overcome the limitations discussed above.

3.2 Requirements definition

In our case, the explanation E for model M that was trained on dataset consisting of features $F \in \{f_1, f_2, \dots, f_n\}$ for an instance x_i is considered to be of the following form given in Equation (1).

$$\Phi^{E \rightarrow M(x_i)} : C(F_1) \wedge C(F_2) \wedge \dots \wedge C(F_k) \rightarrow l \quad (1)$$

Where $C(F_i)$ is a condition in a form of inequality that includes a subset of features $F_i \in F$. In the simple case, F_i will contain only one of the features from F , and $l \in L$ is one of the class labels used by model M .

In the following paragraphs, we define the most important requirements that explanations should meet. We focus on the requirements in the context of rule-based explanations. In our work, we use the definitions of XAI metrics from [40] that we adopted to the needs of a rule-based format.

R1: Simplicity The explanations must be simple in order to be understandable and therefore useful to the expert. The rule-based explanation Φ_1 is considered simpler when Φ_2 if the number of features used to represent Φ_1 is less than the number of features used to represent Φ_2 . Therefore, for $\Phi_1^{E \rightarrow M(x_i)} : C(F_a) \wedge C(F_b) \rightarrow l$ and $\Phi_2^{E \rightarrow M(x_i)} : C(F_i) \wedge C(F_j) \rightarrow l$ the Φ_1 is simpler when Φ_2 if $\|F_a \cap F_b\| < \|F_i \cap F_j\|$. Simple explanations are more comprehensible for users and therefore more useful.

R2: Counterfactual and representative The explanation must provide a counterfactual explanation, preferably in the form of an example from the original dataset. The counterfactual explanation \bar{E} for model M that was trained on dataset consisting of features $F \in \{f_1, f_2, \dots, f_n\}$ for an instance x_i is considered as \bar{x}_i which satisfies the rule given in Equation(2).

$$\Phi_{CF}^{\bar{E} \rightarrow M(x_i)} : C(F_1) \wedge C(F_2) \wedge \dots \wedge C(F_k) \rightarrow \neg l \quad (2)$$

Where $C(F_i)$ is a condition in a form of inequality that includes a subset of features $F_i \in F$ and $\neg l \in L$ is one of the class labels used by the model M , but different than l .

The counterfactual explanation should also be representative, meaning that it should provide a representative example (or examples) from the dataset, otherwise it might be counterintuitive for the expert. This may happen when the counterfactual explanation covers an input space which is populated only with artificial samples, which existence is not possible in real world, due to some constraints that are not captured by the model (like physical constraints).

R3: Consistency and stability The explanation is considered consistent with other explanation methods if it uses the same set of attributes in the same way. Therefore, for two rule-based explanations $\Phi_1^{E \rightarrow M(x_i)} : C(F_a) \wedge C(F_b) \rightarrow l$ and $\Phi_2^{E \rightarrow M(x_i)} : C(F_i) \wedge C(F_j) \rightarrow k$, the explanations are consistent with each other if $k = l$ and $\|(F_a \cap F_b) \cup (F_i \cap F_j)\|$ is maximal and $J(D_1, D_2) = \frac{\|D_1 \cap D_2\|}{\|D_1 \cup D_2\|}$ is maximal, where D_i is a subset of dataset covered by the rule defined by Φ_i and $J(D_i, D_j)$ is a Jaccard index for sets D_i and D_j . In other words, the two rule-based explanations are consistent with each other if they use the same set of attributes to describe the same subset of data. Stability is considered a consistency of rules generated for the same or similar instances by the same explainer in consecutive runs. In other words, the explainer is stable if it generates consistent explanations for similar instances.

R4: Quality-assessment measures Explanations must provide some means of quality assessment to allow the expert to quantify its reliability. One of the basic quality measures applied to the explanation is fidelity. The explanation is considered of high fidelity if $\Phi^{E \rightarrow M(x_i)} = M(x_i)$, meaning that the explanation provides the same prediction for an instance as the original model. Therefore, it shows to what degree the explainer is able to correctly mimic the behavior of a model in a local neighborhood of an instance that is being explained. The fidelity is usually expressed in terms of local and global fidelity. The fidelity itself can be any ML-related metric such as accuracy, F1, precision, recal, etc. For rule-based explainers, local fidelity computes the metric only on a subset of data covered by the explanation rule defined by $\Phi_1^{E \rightarrow M(x_i)}$. Global fidelity is calculated on the larger subset of data, not limited by the coverage of the explanation rule. It can be the whole test set, or some specified neighborhood of the instance that is being explained.

R5: Visual representation The explanation in addition to the quality assessment metrics must be understandable for the addressee. In our previous works [41,

42, 43], we encountered this issue several times when working with domain experts. Even with the extensive explanations provided by the most popular XAI algorithms, they had difficulty in spotting the real mechanics that drive the model towards certain decisions. Therefore, presenting explanations at the semantic level, aligned with the conceptual profile of the addressee of the explanations (the human), is crucial for improving understandability of XAI models for non-technical users. As mentioned previously, understandability can be improved by choosing the representation of explanations that improves the ability of the users to perceive the knowledge gained by a model [44] such as a rule-based explanation [9]. Another direction of research involves studies related to the application of visual explanatory methods. Most of the works in this area focus on the visual presentation of such results, which has been proven to be one of the most effective channels for communicating knowledge in the field of XAI and ML [38, 39]. Work on visualization of explanations includes saliency maps for deep neural networks [45], task-specific visualizations [38, 46], as well as the various plots offered by SHAP and LIME.

In the next Section, we introduce Local Unvertain Explanation (LUX) mechanism – a novel method for generating rule-based factual and counterfactual explanations that addresses all of the aforementioned requirements and issues.

4 Local Universal Explanations

In order to solve the issues of the existing state-of-the-art approaches and fulfill the requirements R1-R4, we propose an algorithm consisting of three phases.

Phase 1 Representative data selection and minimal data generation. Our goal was to explain the decision of the model using the majority of the original data. Therefore, we focused on identifying a representative neighborhood of the instance that is being explained. The generation of samples is reduced to the minimum. This contributes to the simplicity and consistency (stability) of an explanation.

Phase 2 Creation of an explainable rule-based model that is consistent with feature-attribution XAI algorithms (e.g. SHAP or LIME), provides consistent, example-based counterfactuals, and includes uncertainty of the black-box model in both factual and counterfactual explanations. This contributes to simplicity, consistency, and quality assessment requirements.

Phase 3 Explanation visualization. We transferred the weight of the explanation from textual form to visual form. In particular, the rules we generate can

contain two-dimensional linear inequalities, which are hardly comprehensible in text format but difficult to grasp in visual form. This contributes to simplicity and visualization requirements.

4.1 Representative data selection

The problem of selection of representative sample of data to train a local explainer is non trivial task. As discussed before and shown in Figure 2, the state-of-the-art rule-based explainers use artificially generated data as a base for selecting representative sample for training, which corrupts the distribution of the data and makes it difficult to identify the correct neighborhood for local explanations. This may result in overcomplicated explanations and non-truly local explanations, which could be valuable in debugging a ML model, but less informative for domain experts who are mostly interested in what concepts (patterns) in the data are used by the model to provide a certain decision. This question cannot be answered with artificially generated data that domain experts are not familiar with or whose existence in the real world is disputable.

In our method, we wanted to build an explainable model based on concepts that are already there in the data. We noticed that high-density areas of the input space can be considered as prototypes or concepts that can be used to explain the classification. We used OPTICS [47], a density-based clustering algorithm that provides correct results if the distribution is the same as in the case of the original data. Therefore, we inverted the process of selecting a sample for the explanation mechanism compared to the state-of-the-art approaches. We first select the prototype concepts around the neighborhood of the instance that is being explained, based on the original data, and then, if necessary, we generate additional samples to balance the dataset or to resolve the uncertain decision boundaries. For data generation, we modified the BorderlineSMOTE [48] algorithm to up-sample only isolated (surrounded by the opposite class) and uncertain instances (instances for which the blackbox model prediction confidence is low). In the following paragraphs, we describe this process in detail.

Let us assume that an instance for which a decision of a model is to be explained is defined as x_i , and the label of the instance predicted by a blackbox model $M(x_i) = l$. We start by generating a base neighborhood N of size K , which will become a seed for the density-based neighborhood creation method. We define the base neighborhood N of size K as presented in the Equation (3).

$$N^b(x_i, K) = \left\{ \forall_{c \in C}, x_k \in X : \epsilon \geq d(x_i, x_k) \leq D_{i,c}^{(\frac{K}{\|C\|})} \right\} \quad (3)$$

Where $D_{i,c}^{(l)}$ is l -th element from a tuple $D_{i,c}$ defined for all m instances from a

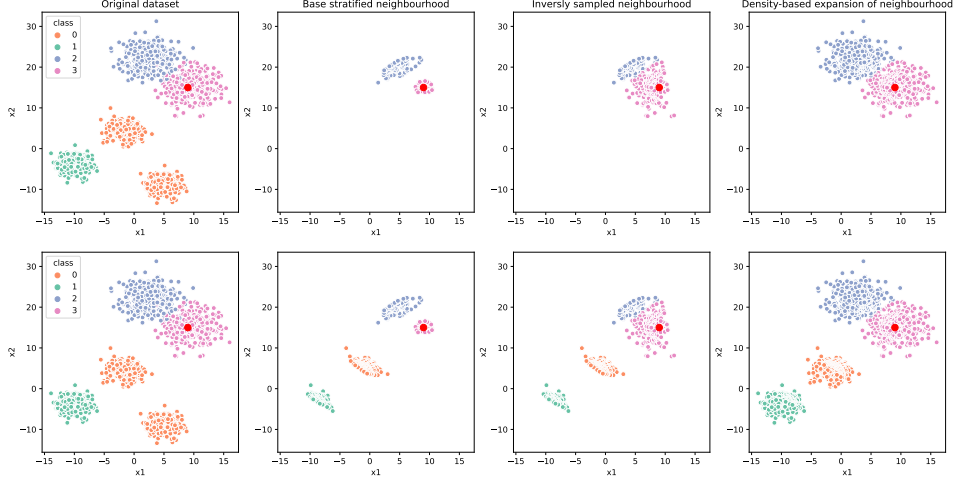


Figure 6: Visualization of a neighborhood selection process in LUX. The upper row shows the selection of the neighborhood according to local stratification and the bottom row shows the process for global stratification. Consecutive plots show consecutive steps of selecting neighborhood.

training set that were labeled as c by a blackbox model M :

$$D_{i,c} = \{d(x_i, x_1), d(x_i, x_2), \dots, d(x_i, x_m)\}$$

$D_{i,c}$ is sorted in ascending order, and $d(x_i, x_j)$ is a distance between instances i -th and j -th. The base neighborhood $N^b(x_i, K)$ is created in a stratified way to ensure the existence of the desired class representatives. The ϵ defines a stratification threshold. The stratification can be local or global, as depicted in Figure 6. In the local stratification, the data is sampled in a range defined by a distance from the instance being explained to the nearest instance of the opposite class. This stratification is desired in the case of simple local explanations and local counterfactuals. In the global stratification, samples from all classes are sampled to become a part of the $D_{i,c}$ training set and the $\epsilon = \infty$ this stratification is more appropriate if counterfactuals should cover a whole spectrum of possible classes.

In addition to stratification, the inverse sampling strategy is also applied. Inverse sampling allows us to better spot the decision boundaries between classes. In this approach, $N^b(x_i, K)$ is extended by $N^{-1}(x_k, K)$ defined in the Equation (4).

$$N^{-1}(x_k, K) = \left\{ x_k \in X : M(x_i) = l, d(x_k, x_i) \leq D_{i,l}^{\left(\frac{K}{\|C\|}\right)} \right\} \quad (4)$$

In other words, the neighborhood is extended with points that surround the decision

boundary that divides the classes $M(x_i) = l$ and $M(x_k) = c$, where l is the class of an instance being explained. The inverse sampling strategy is depicted in Figure 6 in the third column of the plots.

Up to this point, the neighborhood was constructed solely on the basis of the distances between samples. However, such an approach does not take into account the density of the data, which could affect the way the locality is perceived. In particular, high-density areas that were not included in the distance-based neighborhood creation step may contain a significant mass of samples that influences the shape of the decision boundary. This situation is presented in Figure 6 in the last column of the plots. To address this issue, we perform a density-based clustering on the entire training dataset, to obtain a set of n high-density areas of instances $\{C_1, C_2, \dots, C_n\}$. The number of n is governed by the parameter σ which defines a minimal number of instances that can be used to form a cluster (standalone high-density area). Then, we extend the base neighborhood to contain only the sets of these high-density areas that already have some nonempty intersection with points from base neighborhood. Therefore, the final neighborhood N is now defined as:

$$N = N^b \cup N^{-1} \cup \left\{ C_{i=1,2,\dots,n} : C_i \cap \left\{ N^b \cup N^{-1} \right\} \right\} \neq \emptyset \quad (5)$$

Finally, the oversampling algorithm is used to balance the dataset and to generate samples in regions that are highly uncertain. This method does not populate empty regions with artificially generated data like LORE or EXPLAN, but tries to upsample data within the limits defined by the neighborhood N . We extended the BorderlineSMOTE algorithm, which originally generates synthetic samples only around samples called *in-danger*. The *in-danger* sample was a sample whose K -nearest neighbors were from the opposite class. We exploit the observation that the areas which require data generation are those located around the decision boundary. The exact location of decision boundary in multidimensional, non-linear case is non-trivial task, however, its location can be approximated by the confidence of a prediction of the blackbox model. If the prediction of a black-box model is uncertain for a sample x_i it means that the sample is located somewhere in proximity of a decision boundary. Therefore, in our case, we marked all samples x_i , which class label probability returned by the blackbox model were below a threshold t as *in-danger* samples, and followed the original upsampling procedure proposed in BorderlineSMOTE [48]. In our implementation, we used the threshold t to be equal to one standard deviation away from the mean of the confidence of a black-box model. In other words, if we define $P_M(x_i)$ as the confidence of a model M in classifying the sample x_i , the threshold δ is defined as follows:

$$\delta = E[P_M] - \sqrt{E[P_M^2] - E[P_M]^2}$$

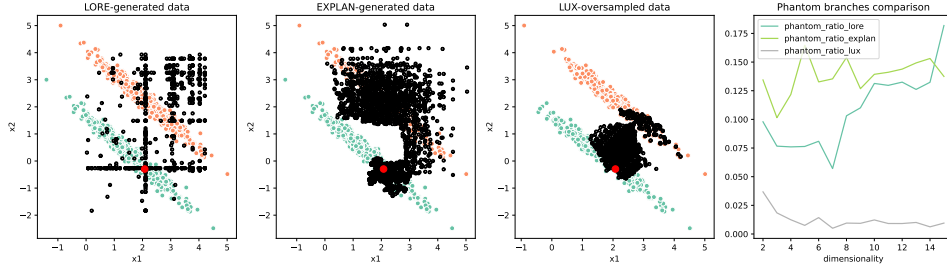


Figure 7: Comparison of the LUX oversampling method with the LORE and EXPLAN approaches. The black circles represent artificially generated data. The red dot represents the instance that is being explained. The colored points represent the original data labeled by the blackbox model.

Additionally, to enforce that the samples are generated only towards the directions that are the most important from the perspective of feature-importance attribution explanation mechanism such as SHAP, we generate samples by transforming existing instances by a vector defined as a negative gradient of the SHAP values. The motivation behind that procedure is in the theoretical justification of SHAP values, which show the impact the feature value of an instance has with respect to the expected value of a blackbox model. While the expected value of a blackbox classification model for a balanced dataset is located around the decision boundary, the analysis of the gradients of SHAP values provides a convenient way of selecting a direction into which the nearest decision boundary might be located without the need of sampling large number of artificial datapoints. The example of this mechanism is depicted in Figure 7, where black circles represent the replicated data in the direction of negative gradients of the SHAP values.

The example of this upsampling is presented in Figure 7. It can be seen that the upsampling does not change the shape of a distribution drastically, not affecting the phantom-branches issue discussed earlier.

The whole neighborhood selection process is governed by two main parameters: K , and σ . The former defines the size of the base neighborhood N^b , and therefore can be used to balance between local and global explanations. The value of K equal to 1 makes the model behave like a global explainer. The latter defines the minimal size of density clusters that are formed to extend the $N^b \cup N_1$ neighborhood. The larger the parameter σ , the stronger the expansion of the base neighborhood. Similarly as in the case of the K parameter, larger values of σ make the model generate less fine-grained local explanations.

The representative sample selection phase tries to find a balance between the local and global neighborhood to select the minimal neighborhood required to gen-

erate explanations that are influenced by high-density areas of the original data points, not local artificially generated masses. This addresses R1 (simplicity) because the neighborhood never gets more complicated than in the original data, and R3 (stability) because the neighborhood selection process is deterministic.

In the following section, we will show how we modified the tree learning algorithm in order to exploit the feature-importance explanation for obtaining simpler, more consistent and stable rule-based explanations.

4.2 Creation of a rule-based explanation model

The neighborhood selected according to the procedure described in previous sections is then used to build explainable rule-based model. The model provides both factual and counterfactual explanations that are consistent (stable) with each other, because they are based on the same tree-based structure, where both factual and counterfactual explanations are single branches extracted from that tree. For the tree generation method, we redesigned the UnertainDecisionTree classifier (UID3) [49, 50] algorithm adding the following extensions: 1) use of the feature-importance explanation model as a support method to select the optimal split, 2) incorporation of oblique splits [51] to better capture decision boundaries of the blackbox model that are linear combinations of several attributes.

We based our method on the UID3 algorithm, by extending notion of information gain split criterion. The classic information gain formula for the numeric feature F and a training set X is defined as follows:

$$Gain(F, X, v) = H(X) - \left[\frac{\|X_{<v}\|}{\|X\|} H(X_{<v}) + \frac{\|X_{\geq v}\|}{\|X\|} H(X_{\geq v}) \right] \quad (6)$$

Where $X_{<v}$ is a subset of $X = \{x_i \in X : x_i < v\}$ and $H(X)$ is the entropy for the training set X is defined as follows:

$$H(X) = - \sum_{l \in Domain(F_t)} p(l) \log_2 p(l) \quad (7)$$

Where $Domain(F_t)$ is a set of all classes in X and $p(l)$ is a ratio of the number of elements of class label l to all the elements in X .

We extended the Equation (6) to include feature importance parameter that allows selection of split attributes that are more consistent with what the original model considers important. It also allows one to overcome the greediness of the decision tree algorithm, because the feature importance values can be considered as the look-ahead parameters [52] that favor the optimal split attributes first. The modified information gain is given as a product of the information gain $Gain(F, X, v)$

Algorithm 1 Split selection algorithm for LUX explanation method.

Input: data X ; set of features F ; balckbox model M
Output: split expression E ; split attribute F_s
if Homogeneous(X) **then**
 return \emptyset
end if
 $F_i, v \leftarrow$ Best split attribute and value using $Gain^{LUX}(F, X, v)$
 $F_{SVM} \leftarrow \{F_1, F_2 \in F : \max(Imp(F_1) + Imp(F_2))\}$
Train linear SVM classifier on X and F_{SVM}
 $V_{F_1} \leftarrow \alpha F_2 + \beta$ as a decision boundary or SVM
if $Gain^{LUX}(F_i, X, v) < Gain^{LUX}(F_1, X, V_{F_1})$ **then**
 $E \leftarrow \alpha F_2 + \beta$
 $F_s \leftarrow F_1$
else
 $E \leftarrow v$
 $F_s \leftarrow F_i$
end if
return split expression E ; split attribute F_s

and the importance of the feature F_i . The formula is given in Equation (8).

$$Gain^{LUX}(F_i, X, v) = Gain(F_i, X, v) \cdot Imp(F_i) \quad (8)$$

Where $Imp(F_i)$ is the average absolute importance of feature F_i returned from feature-importance explanation mechanism such as SHAP or LIME.

We also added the oblique splits, which allow us to create a split in decision tree that contains a condition which is a linear combination of several features. In our approach we limited the oblique splits to use only two features because this allows us to visualize splits as 2D scatterplots. The complete procedure for selecting an attribute and an expression to create a split in the decision tree was presented in Algorithm 1.

The procedure is called recursively during the tree-building algorithm. At a given depth of a tree, the expression E and the attribute F_s returned by Algorithm 1 are used as building blocks of a decision tree. The F_i becomes a tree node, and the expression E is used as the right-hand side of a condition on a tree branch originating at node F_i . The condition is denoted as $C(F)$, where F is a set containing both the split feature F_i and other features that can be part of expression E . Finally, the explanation $\Phi^{E \rightarrow M(x_i)}$ as defined in Equation (1) is extracted from a tree as a conjunction of $C(F)$ that the explained instances pass through the tree during the classification process.

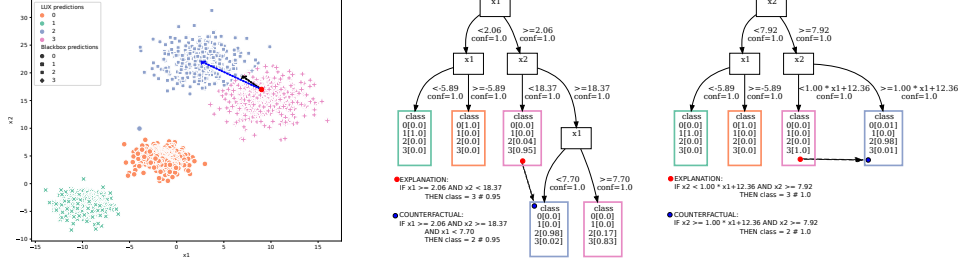


Figure 8: Illustrative example of explanation generation with classic method (left tree) and shap-enhanced oblique splits we proposed. The arrow in the scatterplot represent the counterfactual explanations generated with right tree. The black arrow shows classical counterfactual example, the blue arrow shows medoid-based counterfactual example.

The example of explanations generated with the LUX algorithm is given in Figure 8. The left decision tree was generated using the classical method, and the right decision tree was generated with the use of SHAP feature importances and oblique splits. The latter is less complex (in terms of depth) and of better quality (in terms of classification accuracy). The explanation $\Phi^{E \rightarrow M}(x_i)$ for $x_i = [9, 15]$ is created by extracting a tree branch ending in a leaf that contains the instance x_i .

The same tree structure is used to generate counterfactual explanations. This ensures that the counterfactual explanation is consistent with the factual explanation in terms of the features used in a rule. The counterfactual explanation $\Phi_{CF}^{\bar{E} \rightarrow M}(x_i)$ as defined in Equation (2) is an explanation that tells how the given instance should change in order to be classified differently by the blackbox model. Therefore, in a first step to generate counterfactual explanation for an instance x_i , we search all branches in the explanation tree that have a leaf with majority of samples labeled differently than the x_i . In the second step, we search for the nearest neighbor in instances covered by different branches. The instance \bar{x}_i that is the nearest neighbor of x_i becomes a counterfactual example, and the tree branch that contains the \bar{x}_i becomes the explanation $\Phi_{CF}^{\bar{E} \rightarrow M}(x_i)$. Alternatively, to nearest neighbor one can search for the nearest medoid instead of the nearest instance. In such a case, the $\Phi_{CF}^{\bar{E} \rightarrow M}(x_i)$ is generated based on the branch of the explanation tree that covers a set of instances which medoid is the nearest neighbor of instance x_i . In this setting, the medoid becomes the counterfactual example \bar{x}_i . In Figure 8 both types of counterfactuals were visualized with arrows: the black represents the nearest-neighbor counterfactual, while the blue represents the medoid-based counterfactual.

Although the explanations generated with LUX are simpler (R1) and provide better quality in terms of fidelity compared with state-of-the-art methods, usability might be limited due to the difficulty in oblique splits comprehension. In the next section, we describe how we overcome this problem by enabling simple visualizations of explanations to make them more understandable and useful.

4.3 Explanation visualization

The explanation has to be understandable by the user in order to present some value in practical applications. In this section, we present a visualization layer that we included in our LUX explainer. Because our explanation method is based on decision trees, we focused on visualizing this component. The visual representation of an explanation tree from Figure 8 was presented in Figure 9. It follows the standard structure of the tree, with nodes representing features and edges representing split conditions. However, the nodes do not only contain the name of the feature, but also present the data distribution and a location of a split in this context (the red dotted line). In case of oblique splits, we present the node in 2D with a linear boundary representing the split.

The visualization we propose makes the explainability process more human-readable and the explanation itself more informative. For example, consider the explanation in a rule format, as it was presented in Figure 8:

```
IF x2 < 1.00 * x1+12.36 AND x2 >= 7.92 THEN class = 3 # 1.0
```

It is hardly possible to actually understand the explanation without additional context, such as the possible ranges of values for feature x_2 . The visualization of this context in a form of distribution plot, with marked location of explained instance, allows the user to immediately generate counterfactuals, without any sophisticated methods. For example, only by looking at the first split, one can notice that in order to flip decision of the model from class 3 to class 0 it is enough to change the value of x_2 to 5 and the value of x_1 to any value from a range of $(-5; 2.5)$. Such an operation would not be possible with only the textual version of the explanation.

Furthermore, the visualization of distribution allows for expert-based quality assessment of the explanation and counterfactual. For example, if the counterfactual explanation was located very close to the decision boundary in a scatterplot in Figure 9, one can immediately judge this explanation as uncertain and even manually correct it by pushing the values of the counterfactual further away from the decision boundary. Such a modification would not be possible with a textual explanation.

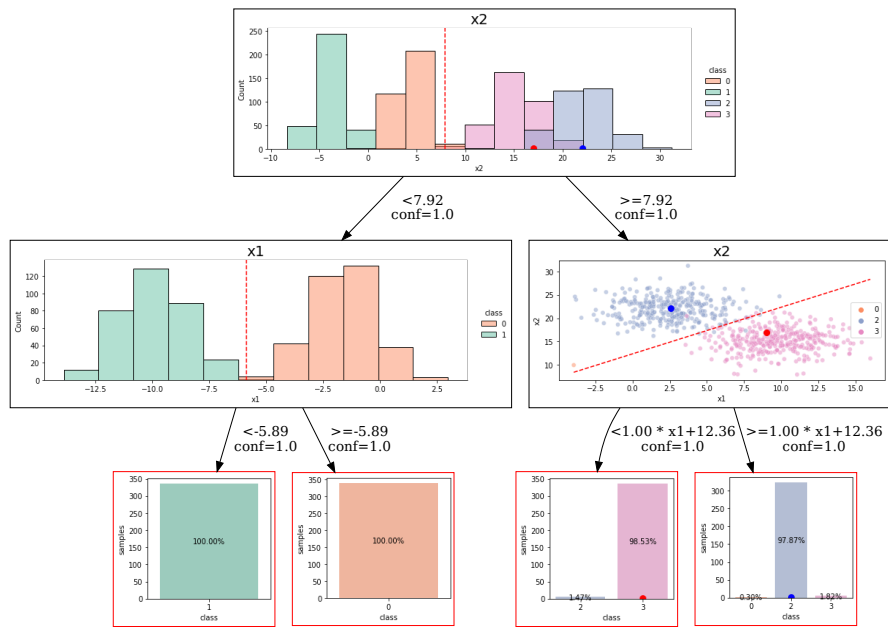


Figure 9: Visual representation of an explanation tree presented in Figure 8. It embeds information about data distribution at different levels of the tree and visualizes the path that explained instance (red dot) and medoid-based counterfactual passes through the tree.

Table 1: Description of the real datasets we used for evaluation.

Dataset name	No of instances	No of features	Class ratio
house_16H	13488.00	16.00	0.50
wine	2554.00	11.00	0.50
ipums-small	5188.00	20.00	0.50
phoneme	3172.00	5.00	0.50
california	20634.00	8.00	0.50
bank-marketing	10578.00	7.00	0.50
jannis	57580.00	54.00	0.50
MagicTelescope	13376.00	10.00	0.50
eye_movements	7608.00	20.00	0.50
credit	16714.00	10.00	0.50
pol	10082.00	26.00	0.50
cancer	569.00	30.00	0.63
electricity	38474.00	7.00	0.50

5 Evaluation

In this section, we present results from our evaluation of the LUX explainer. We used synthetic datasets in cases where we investigated impact of the size of the dataset, and number of features on the explainability method. In other cases, we used real, publicly available data.

Our evaluation approach was aimed at investigating the performance of LUX with respect to the previously defined four requirements R1-R4. We compared our method with the most popular rule-based explainers discussed previously: LORE, EXPLAN and Anchor.

Our main goal was to show that we can achieve simpler, more consistent rules and counterfactuals without affecting the fidelity of the explainer. In comparing the explainers, we used 13 real dataset and several different sets of synthetic datasets, depending on the evaluation task. See Table 1 for details of each of the real dataset.

First, we collected results from all the explainers performed on the same datasets for the same instance. Then, we performed a Friedman test followed by a Nemenyi pairwise post-hot test for multiple comparisons of mean rank sums. This allowed us to observe how the algorithms differ, and between which algorithms the difference is statistically significant. We excluded Anchor from comparisons that involved evaluation of features that this particular explainer does not offer (e.g. counterfactuals). The results of the evaluation are presented below.

Table 2: Results from the experiments on local fidelity. The value after \pm corresponds to standard deviation.

Dataset	LUX	EXPLAN	LORE	Anchor
cancer	0.98 ± 0.07	0.96 ± 0.13	0.95 ± 0.13	0.97 ± 0.14
MagicTelescope	0.84 ± 0.21	0.80 ± 0.19	0.82 ± 0.14	0.81 ± 0.18
bank-marketing	0.79 ± 0.22	0.80 ± 0.18	0.82 ± 0.08	0.84 ± 0.11
california	0.92 ± 0.10	0.86 ± 0.18	0.85 ± 0.11	0.86 ± 0.17
credit	0.79 ± 0.16	0.78 ± 0.13	0.82 ± 0.08	0.80 ± 0.19
electricity	0.84 ± 0.16	0.82 ± 0.15	0.83 ± 0.10	0.73 ± 0.29
eye_movements	0.61 ± 0.26	0.57 ± 0.21	0.65 ± 0.17	0.62 ± 0.09
house_16H	0.83 ± 0.27	0.87 ± 0.15	0.90 ± 0.08	0.82 ± 0.32
jannis	0.76 ± 0.23	0.74 ± 0.19	0.76 ± 0.16	0.82 ± 0.11
ipums-small	0.90 ± 0.15	0.89 ± 0.12	0.89 ± 0.09	0.85 ± 0.29
phoneme	0.79 ± 0.25	0.80 ± 0.19	0.84 ± 0.11	0.84 ± 0.14
pol	0.95 ± 0.16	0.94 ± 0.15	0.96 ± 0.05	0.28 ± 0.43
wine	0.81 ± 0.17	0.76 ± 0.21	0.80 ± 0.11	0.83 ± 0.11

5.1 Fidelity

The first phase of evaluation aimed in comparing local fidelity of LORE, EXPLAN, Anchor and LUX on various datasets to observe if our explainer provides comparable results to other methods. As a measure of fidelity, we used the F1 score and tested it on the real datasets introduced in Table 1. In this test, the higher the value of fidelity, the better. For each dataset we randomly selected 100 instances and generated explanations for them with each of the evaluated explainers. For instances in which the explainer could not generate any explanation, the fidelity was set to 0. The results are presented in Table 2. We used these results to perform statistical tests to prove that there is no difference in local fidelity between any of the explainers. From Friedman test, we obtained statistics equal to 7.15, with p-value equal to 0.06. With 13 datasets and 4 algorithms we had 3 and 36 degree of freedom respectively, which allowed us to determine that the critical value for $F(3, 36)$ for $\alpha = 0.05$ is 2.87. This allowed us to reject the null hypothesis. After that we performed the Nemenyi test to observe how the algorithms differ and if the difference is statistically significant. The results of that test and the critical distance are visualized in Figure 10.

Based on that, we can conclude that the local fidelity differences are not statistically significant between the explainers. The next step was to check the results for other properties such as simplicity, counterfactuals' fidelity, etc.

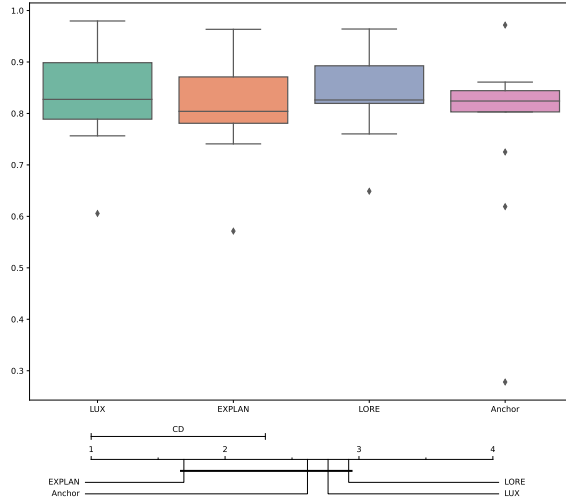


Figure 10: Visualization of the results represente in Table 2 (top figure) and Nemenyi post-hoc test results (bottom figure) with critical distance marked as hirizontal bold line. The higher the better.

5.2 Simplicity

In tests for simplicity, we investigated whether we can obtain shorter rules without affecting the quality of the explainer model. The length of the rules was calculated as the number of different attributes used in the conditions of a rule. In this test, the smaller the value the better, therefore in the Nemenyi test, the lower the rank, the better. It can be seen that LUX produces significantly simpler rules explanations than other explainers, as depicted in Table 3 and Figure 11.

From the Friedman test, we obtained statistics equal to 10.75, ith p-value equal to 0.009. We used the same set of data sets as previously, therefore, for $\alpha = 0.05$ the critical value is 2.87, which allows us to reject the null hypothesis.

5.3 Consistency and stability

We tested the consistency with SHAP values of all of the explainers. We calculated the consistency as an average SHAP importance of attributes used in rules by different explainers. We tested this property on real datasets. The results are presented in Table 4 and visualized in Figure 12. Although from the statistical test it is visible that the differences are statistically irrelevant for all of the explainer, LUX got one of the highest ranks among all of the methods.

We tested the stability of the explanations by calculating the Jaccard index for

Table 3: Results of simplicity test performed on real datasets. The lower the value, the better.

Dataset	LUX	EXPLAN	LORE	Anchor
cancer	2.45 ± 0.95	4.82 ± 1.34	3.63 ± 1.48	2.66 ± 0.64
MagicTelescope	3.38 ± 1.07	3.88 ± 1.38	3.75 ± 1.78	5.18 ± 4.18
bank-marketing	2.75 ± 1.19	3.19 ± 1.19	2.66 ± 1.39	3.60 ± 2.31
california	3.20 ± 0.85	3.31 ± 0.88	3.19 ± 0.93	3.84 ± 2.11
credit	3.72 ± 1.26	4.36 ± 1.39	3.74 ± 1.93	4.07 ± 2.47
electricity	2.23 ± 0.81	2.25 ± 0.73	1.84 ± 1.09	3.94 ± 2.82
eye_movements	5.88 ± 1.71	5.67 ± 1.83	5.60 ± 2.36	2.23 ± 0.98
house_16H	4.07 ± 1.22	4.57 ± 1.32	4.11 ± 1.64	3.23 ± 0.91
jannis	4.46 ± 1.41	5.12 ± 1.46	4.50 ± 2.19	2.77 ± 0.81
ipums-small	2.55 ± 1.21	3.76 ± 1.39	3.49 ± 1.45	2.78 ± 1.59
phoneme	3.51 ± 0.95	3.37 ± 0.92	3.15 ± 1.03	5.26 ± 2.16
pol	2.04 ± 1.22	3.36 ± 1.31	3.14 ± 2.04	6.31 ± 4.44
wine	3.56 ± 1.35	4.19 ± 1.51	4.24 ± 1.99	3.58 ± 1.92

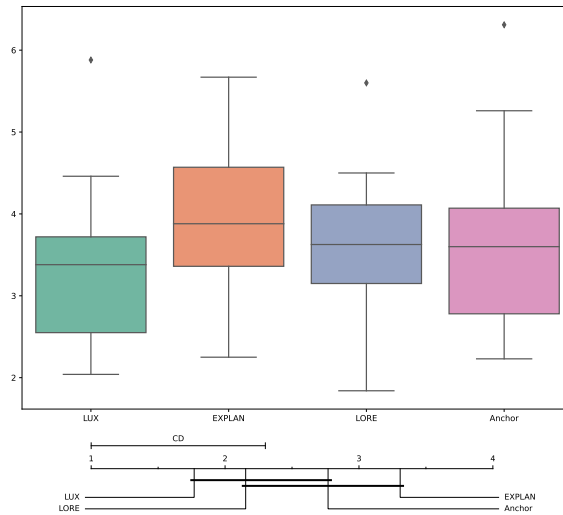


Figure 11: Visualization of the results for simplicity tests presented in Table 3 (top figure) and Nemenyi post-hoc test results (bottom figure) with critical distance marked as horizontal bold line. The lower the better.

Table 4: Results of consistency with SHAP test performed on synthetic datasets. The higher the value, the better.

Dataset size	LUX	EXPLAN	LORE	Anchor
cancer	0.10	0.10	0.12	0.08
MagicTelescope	0.26	0.19	0.23	0.19
bank-marketing	0.36	0.29	0.38	0.30
california	0.27	0.24	0.27	0.22
credit	0.22	0.16	0.24	0.22
electricity	0.43	0.42	0.54	0.32
eye_movements	0.12	0.10	0.12	0.18
house_16H	0.15	0.12	0.14	0.14
jannis	0.13	0.09	0.12	0.14
ipums-small	0.23	0.18	0.21	0.20
phoneme	0.24	0.24	0.26	0.18
pol	0.56	0.32	0.42	0.18
wine	0.20	0.15	0.18	0.18

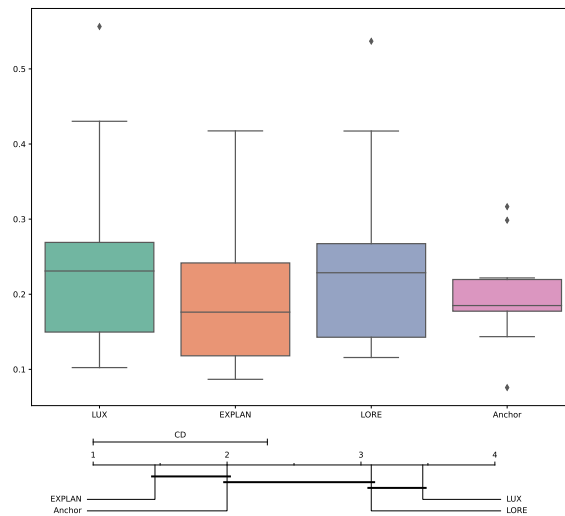


Figure 12: Visualization of the results for consistency with SHAP tests presented in Table 4 (top figure) and Nemenyi post-hoc test results (bottom figure) with the critical distance marked as horizontal bold line. The lower the better.

Table 5: Results of stability test performed on synthetic datasets. The higher the value, the better.

Dimensionality	LUX	EXPLAN	LORE	Anchor
4	1.00	0.68	0.86	0.83
5	0.99	0.66	0.96	1.00
6	1.00	0.65	0.89	1.00
7	0.98	0.64	0.91	0.99
8	0.98	0.59	0.61	0.77
9	0.64	0.53	0.72	0.88
10	0.61	0.64	1.00	0.84
11	0.66	0.63	0.82	0.89
12	0.99	0.40	0.78	0.92
13	0.96	0.46	0.82	0.98
14	0.62	0.45	0.66	0.69
15	0.66	0.42	0.56	0.70
16	0.65	0.36	0.51	0.83
17	0.42	0.42	0.66	0.50
18	0.65	0.37	0.55	0.96

the set of features used in consecutive calls of explanation for the same instance. The different configurations of datasets were selected to observe the relation between the number of features, size of the dataset, and size of noise (non-informative features) to the stability of explanations. The results are presented in Table 5 and visualized in Figure 13. It can be seen that although the best performing algorithm in this test is LUX.

We also conducted tests on stability in real data. Because we could not manipulate the data as in the case of synthetic datasets, we used a metric that is based on Local Lipschitz Continuity metric [53]. It expresses to what extent the explanations for similar observations similar to each other. It is calculated as the ratio of instances covered by the explainable rule to the distance between two instances that are explained. The higher the value, the better.

The results are presented in Table 6 and visualized in Figure 14.

5.4 Counterfactuals and representativeness

Due to the fact that only LORE provides the explicit way to generating counterfactual explanations, we tested this requirement by checking the number of phantom branches present in the data. Additionally, we used global fidelity of the explana-

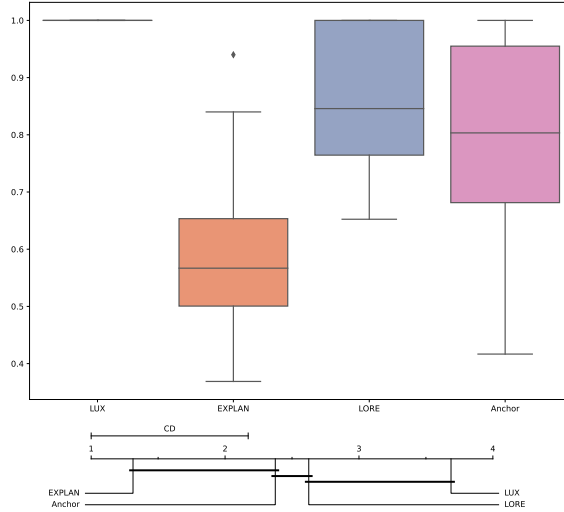


Figure 13: Visualization of the results for stability tests presented in Table 5 (top figure) and Nemenyi post-hoc test results (bottom figure) with critical distance marked as horizontal bold line. The higher the better.

Table 6: Results of stability test performed on real datasets. The higher the value, the better.

Dataset	LUX	EXPLAN	LORE	Anchor
cancer	0.25	0.33	0.27	0.16
MagicTelescope	0.53	0.40	0.40	0.38
bank-marketing	0.53	0.50	0.50	0.42
california	0.67	0.61	0.64	0.46
credit	0.58	0.42	0.40	0.43
electricity	0.59	0.58	0.63	0.46
eye_movements	0.48	0.34	0.29	0.33
house_16H	0.41	0.39	0.35	0.29
jannis	0.36	0.27	0.28	0.31
ipums-small	0.36	0.45	0.43	0.32
phoneme	0.59	0.54	0.52	0.61
pol	0.40	0.49	0.34	0.31
wine	0.38	0.36	0.36	0.32

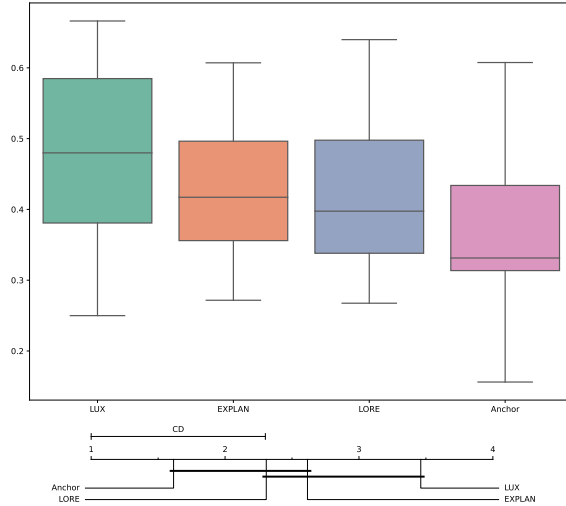


Figure 14: Visualization of the results for stability tests presented in Table 6 (top figure) and Nemenyi post-hoc test results (bottom figure) with the critical distance marked as horizontal bold line. The higher the better.

tion trees of LORE, EXPLAN and LUX as an approximation of an average fidelity of all possible counterfactuals. To measure the global fidelity, we used the F1 score, as in case of local fidelity. We excluded Anchor as a method which was not designed to generate counterfactuals.

From the results presented in Table 7 and the statistical tests presented in Figure 15, LUX produces counterfactual explanations that are significantly better than other explainers.

Another interesting observation is that all of the explainers are very different in terms of the quality of counterfactual explanations, although they use exactly the same underlying mechanism for generating rules, which is a decision tree. The main difference between the explainers can be found in the way they generate and select data for training the decision tree. Therefore, the choice of the selection of a representative sample for training is crucial for delivering good quality counterfactual, but is not that important in delivering good quality local explanations.

We also measured the representativeness of counterfactual as a fraction of branches in a decision tree that has zero-coverage in test set (phantom branches). We used for that purpose the synthetic datasets, where we increase the dimensionality and measure the fraction of phantom branches. The results are given in Table 8, where it can be clearly seen that only in the case of LUX the fraction of phantom branches does not increase with the dimensionality and remains at the reasonably

Table 7: Global fidelity of generated rules. It can be considered as an approximation of average fidelity of all possible counterfactuals.

Dataset	LUX	EXPLAN	LORE
cancer	0.98 ± 0.04	0.97 ± 0.06	0.96 ± 0.11
MagicTelescope	0.93 ± 0.07	0.84 ± 0.13	0.81 ± 0.18
bank-marketing	0.96 ± 0.04	0.91 ± 0.08	0.90 ± 0.08
california	0.95 ± 0.02	0.88 ± 0.11	0.82 ± 0.13
credit	0.96 ± 0.03	0.91 ± 0.09	0.88 ± 0.07
electricity	0.97 ± 0.04	0.91 ± 0.10	0.86 ± 0.14
eye_movements	0.81 ± 0.05	0.72 ± 0.08	0.65 ± 0.11
house_16H	0.93 ± 0.06	0.89 ± 0.08	0.84 ± 0.11
jannis	0.92 ± 0.06	0.83 ± 0.12	0.82 ± 0.12
ipums-small	0.98 ± 0.03	0.95 ± 0.07	0.91 ± 0.09
phoneme	0.95 ± 0.05	0.84 ± 0.13	0.86 ± 0.14
pol	0.98 ± 0.02	0.96 ± 0.04	0.94 ± 0.07
wine	0.92 ± 0.05	0.84 ± 0.12	0.80 ± 0.11

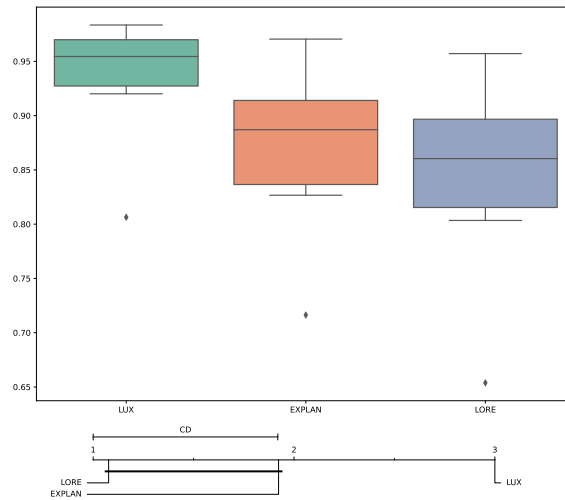


Figure 15: Visualization of the results for counterfactual fidelity tests presented in Table 7 (top figure) and Nemenyi post-hoc test results (bottom figure) with the critical distance marked as horizontal bold line. The higher the better.

Table 8: Results representing fraction of phantom-branches in a explanation tree built by different explainers.

Dimensionality	LUX	EXPLAN	LORE
2	0.04	0.13	0.10
3	0.02	0.10	0.08
4	0.01	0.12	0.08
5	0.01	0.16	0.08
6	0.01	0.13	0.08
7	0.01	0.14	0.06
8	0.01	0.15	0.10
9	0.01	0.13	0.11
10	0.01	0.14	0.13
11	0.01	0.14	0.13
12	0.01	0.14	0.13
13	0.01	0.15	0.13
14	0.01	0.15	0.13
15	0.01	0.14	0.18

low level. Other methods which rely on generating synthetic samples suffer from that issue, which may result in producing counterfactual rules that are impossible to achieve in reality.

5.5 Visualization

Finally, we also tested the visual aspect of the LUX explanations. The goal of this experiment was to check whether there is a difference between the usefulness of explanations provided in the form of rules and visual explanations. We conducted the experiment on 19 participants who had basic knowledge in the area of data science. The participants were divided into two subgroups by random assignments: the first group had access to visualizations (12 participants) of explanations, and the other group did not (7 participants). Both subgroups had to solve the same set of assignments related to three different instances and explanations that were generated for these instances. The assignments included:

1. (Q1) Based on the explanation provided by LUX, try to predict what will be the model output for the given instance.
2. (Q2) Change the counterfactual example that LUX provided in a way that will let you be more certain that it is correct, i.e. increase the confidence of

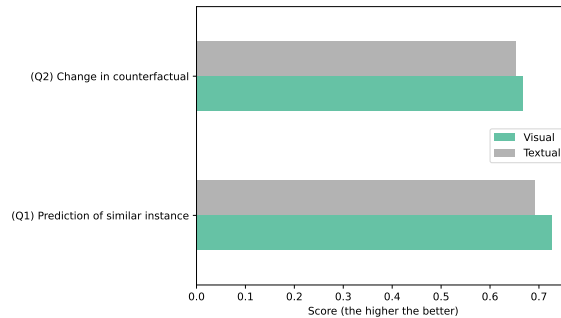


Figure 16: Scores for assignments completed by the participants.

the counterfactual being classified to the opposite class as explained instance.

The final step of the experiment was a short survey that contained following questions:

1. Rate the overall experience of using LUX on a 5-point bipolar scaling method, analogous to the Likert scale.
2. Describe the biggest advantage of LUX
3. Describe the biggest disadvantage of LUX

Additionally, we performed analysis of the assignments that the participants had to solve and measured time of completion of this tasks. Both groups obtained very similar results in all of the assignments and in time of completion. The results for scores obtained for assignments (Q1) and (Q2) were visualized in Figure 16. The scores were calculated as accuracy of human-based prediction (Q1) and accuracy of a blackbox model on a counterfactuals generated by humans (Q2). The completion times were presented in Figure 17.

Furthermore, both groups rated the visual and textual versions of LUX similarly, where the visual version obtained scores equal to 3.62 and the textual version 3.57. The larger differences were observed in descriptions of advantages of tools. The biggest advantage pointed out by the group that had access to the visualization of the explanations was the visual aspect, which proves that it is a feature that users value. The biggest disadvantage was the lack of detailed instructions on how to interpret the explanations. This was a surprising finding, because the rules and decision tree formats were very well known by the participants. It may suggest that the assumption on the simplicity of the way the knowledge is presented to the user is very subjective. Therefore, the explanations should be more contextualized and personalized.

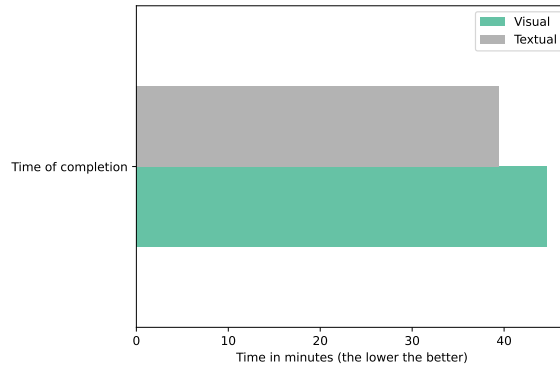


Figure 17: Time of completion for all of the assignments.

5.6 Discussions of the results

In this section, we summarize the results from the evaluation provide their concise interpretation. The summary of these objective metrics is shown in Figure 18. The ranks used in the figure were obtained from average performance from different tests. The average of the ranks that would have been assigned to all the tied values is assigned to each value. Due to the fact that there exists trade-off between different metrics, it is desirable to maximize the area on the radar plot from Figure 18. It can be seen that the largest area is reserved for LUX.

From the experiments we conducted, it is evident that in terms of fidelity, LORE performs better than LUX. However, the differences observed are not statistically significant, and when considering average fidelity values obtained for all of the datasets which are 83.0 for LUX and 83.7 for LORE, the variations are minimal. Furthermore, the counterfactuals generated with LUX exhibit noticeably higher fidelity than any other methods. The rules generated by LUX are the simplest in terms of the number of features used for explanation. In addition, LUX demonstrates the highest SHAP consistency, indicating that it utilizes features that are also important according to the SHAP explainer. This could be attributed to the novel sampling mechanism used, which limits the number of samples and generates samples only in the directions of the largest gradients of SHAP values, pointing toward decision boundaries. Regarding consistency and stability, LUX stands out as the most consistent and stable explainer among all, providing similar explanations for similar instances. This feature enhances the robustness of our explainer and has practical value.

The most surprising results stemmed from the evaluation of visualizations. We observed minimal and statistically insignificant differences in responses between

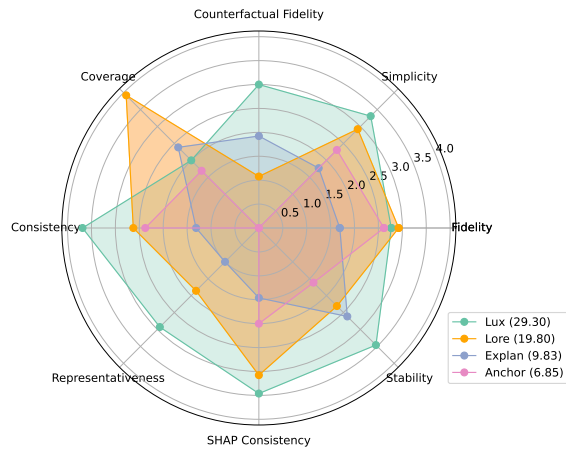


Figure 18: Summary plot of all the metrics used in evaluation. The larger the area for a particular explainer, the better. The number next to the legend is the area of the polygon on the plot defined by the ranks obtained for particular methods.

textual and visual versions of LUX, while comments highlighted a visual feature discrepancy. The comments of the participants in the post-hoc survey revealed that the synthetic nature of the study presented challenges in understanding the explanations. This aspect carried significant weight in the final evaluation, causing participants to concentrate more on difficulties in comprehending the data and the case rather than the explanations themselves. The primary concern was not the manner in which explanations were presented but rather how the information conveyed could have been contextualized by the intended recipients of the explanation. The participants suggested that if the same data and explanations were provided with context, such as meaningful names for features and a description of a real-world case scenario (e.g., loan approval or income prediction), it would be much easier to understand the explanations. This implies the need for a greater involvement of social sciences in XAI research, particularly in investigating the informative competencies of different types of explanation recipients and formulating guidelines for personalizing XAI. This collaborative effort should be a mutual effort between the computer science and social science domains.

6 Summary

In this work, we presented LUX, which is a local universal rule-based explainer that combines factual, counterfactual and visual explanations into one bundle. It

does not depend on synthetic samples, such as other state-of-the-art explainers, but rather focuses on extracting representative clusters of original data to train an interpretable decision tree classifier on top of it. It combines feature-importance explanation methods such as SHAP or LIME to help build more stable decision trees and allows for oblique rules which can capture linear boundaries much better than any other rule-based explainer. From the evaluation on both real and synthetic datasets, we obtained results that prove that LUX performs better in terms of simplicity, representativeness of counterfactuals and counterfactuals' fidelity than core of the state-of-the-art explainers such as LORE, EXPLAN and Anchor without affecting the local fidelity of the explanations. It is also the best algorithm in terms of stability of its explanations among consecutive runs and consistency with SHAP values.

However, it is worth keeping in mind the limitations of LUX. One of the major ones is its computational complexity. For a single explanation, we need to perform three complex steps: calculation of SHAP values, neighborhood selection, and density clustering. It becomes very time- and memory-consuming for large datasets. The second limitation is that LUX depends on the distance measures in the selection of neighborhood. This works well for low-dimensional tabular data, but could be an issue in high-dimensional datasets or in other modalities such as text, images, or time series. In such a case, one has to provide a distance metric that satisfies the different modality (text, images, time-series) or perform dimensionality reduction during neighborhood selection and clustering.

The source code of LUX, notebooks and data used for evaluation are publicly available under the MIT license on <https://github.com/sbobek/lux>.

References

- [1] B. Goodman, S. Flaxman, EU regulations on algorithmic decision-making and a "right to explanation", cite arXiv:1606.08813Comment: presented at 2016 ICML Workshop on Human Interpretability in Machine Learning (WHI 2016), New York, NY (2016).
URL <http://arxiv.org/abs/1606.08813>
- [2] P. Hacker, J.-H. Passoth, Varieties of AI Explanations Under the Law. From the GDPR to the AIA, and Beyond, in: A. Holzinger, R. Goebel, R. Fong, T. Moon, K.-R. Müller, W. Samek (Eds.), *xxAI - Beyond Explainable AI: International Workshop, Held in Conjunction with ICML 2020*, July 18, 2020, Vienna, Austria, Revised and Extended Papers, Lecture Notes in Computer Science, Springer International Publishing, Cham, 2022, pp. 343–

373. doi:10.1007/978-3-031-04083-2_17.
URL https://doi.org/10.1007/978-3-031-04083-2_17

- [3] M. Ghassemi, L. Oakden-Rayner, A. L. Beam, The false hope of current approaches to explainable artificial intelligence in health care, *The Lancet Digital Health* 3 (11) (2021) e745–e750. doi:10.1016/S2589-7500(21)00208-9.
URL <https://www.sciencedirect.com/science/article/pii/S2589750021002089>
- [4] S. Verma, A. Lahiri, J. P. Dickerson, S.-I. Lee, Pitfalls of Explainable ML: An Industry Perspective, arXiv:2106.07758 [cs] (Jun. 2021). doi:10.48550/arXiv.2106.07758.
URL <http://arxiv.org/abs/2106.07758>
- [5] J. Roski, E. J. Maier, K. Vigilante, E. A. Kane, M. E. Matheny, Enhancing trust in AI through industry self-governance, *Journal of the American Medical Informatics Association* 28 (7) (2021) 1582–1590. arXiv:<https://academic.oup.com/jamia/article-pdf/28/7/1582/38983302/ocab065.pdf>, doi:10.1093/jamia/ocab065.
URL <https://doi.org/10.1093/jamia/ocab065>
- [6] T. Evans, C. O. Retzlaff, C. Geißler, M. Kargl, M. Plass, H. Müller, T.-R. Kiehl, N. Zerbe, A. Holzinger, The explainability paradox: Challenges for xAI in digital pathology, *Future Generation Computer Systems* 133 (2022) 281–296. doi:10.1016/j.future.2022.03.009.
URL <https://www.sciencedirect.com/science/article/pii/S0167739X22000838>
- [7] U. Ehsan, M. O. Riedl, Explainability Pitfalls: Beyond Dark Patterns in Explainable AI, arXiv:2109.12480 [cs] (Sep. 2021). doi:10.48550/arXiv.2109.12480.
URL <http://arxiv.org/abs/2109.12480>
- [8] C. Molnar, G. König, J. Herbinger, T. Freiesleben, S. Dandl, C. A. Scholbeck, G. Casalicchio, M. Grosse-Wentrup, B. Bischl, General Pitfalls of Model-Agnostic Interpretation Methods for Machine Learning Models, in: A. Holzinger, R. Goebel, R. Fong, T. Moon, K.-R. Müller, W. Samek (Eds.), *xxAI - Beyond Explainable AI: International Workshop, Held in Conjunction with ICML 2020, July 18, 2020, Vienna, Austria, Revised and Extended Papers*, Lecture Notes in Computer Science, Springer International Publishing,

Cham, 2022, pp. 39–68. doi:10.1007/978-3-031-04083-2_4.
URL https://doi.org/10.1007/978-3-031-04083-2_4

- [9] R. Butz, R. Schulz, A. Hommersom, M. van Eekelen, Investigating the understandability of xai methods for enhanced user experience: When bayesian network users became detectives, *Artificial Intelligence in Medicine* 134 (2022) 102438. doi:<https://doi.org/10.1016/j.artmed.2022.102438>.
URL <https://www.sciencedirect.com/science/article/pii/S0933365722001907>
- [10] R. Gaudel, L. Galárraga, J. Delaunay, L. Rozé, V. Bhargava, s-lime: Reconciling locality and fidelity in linear explanations, in: T. Bouadi, E. Fromont, E. Hüllermeier (Eds.), *Advances in Intelligent Data Analysis XX*, Springer International Publishing, Cham, 2022, pp. 102–114.
- [11] G. Vilone, L. Longo, A quantitative evaluation of global, rule-based explanations of post-hoc, model agnostic methods, *Frontiers in Artificial Intelligence* 4 (2021).
- [12] G. Vilone, L. Longo, A novel human-centred evaluation approach and an argument-based method for explainable artificial intelligence, in: I. Maglogiannis, L. Iliadis, J. Macintyre, P. Cortez (Eds.), *Artificial Intelligence Applications and Innovations*, Springer International Publishing, Cham, 2022, pp. 447–460.
- [13] A. Adadi, M. Berrada, Peeking Inside the Black-Box: A Survey on Explainable Artificial Intelligence (XAI), *IEEE Access* 6 (2018) 52138–52160, conference Name: IEEE Access. doi:10.1109/ACCESS.2018.2870052.
- [14] A. Barredo Arrieta, N. Díaz-Rodríguez, J. Del Ser, A. Bennetot, S. Tabik, A. Barbado, S. Garcia, S. Gil-Lopez, D. Molina, R. Benjamins, R. Chatila, F. Herrera, Explainable Artificial Intelligence (XAI): Concepts, taxonomies, opportunities and challenges toward responsible AI, *Information Fusion* 58 (2020) 82–115. doi:10.1016/j.inffus.2019.12.012.
URL <https://www.sciencedirect.com/science/article/pii/S1566253519308103>
- [15] W. R. Swartout, XPLAIN: a system for creating and explaining expert consulting programs, *Artificial Intelligence* 21 (3) (1983) 285–325. doi:10.1016/S0004-3702(83)80014-9.
URL <https://www.sciencedirect.com/science/article/pii/S0004370283800149>

- [16] Explainable Artificial Intelligence.
URL <https://www.darpa.mil/program/explainable-artificial-intelligence>
- [17] General Data Protection Regulation (GDPR) – Official Legal Text.
URL <https://gdpr-info.eu/>
- [18] Proposal for a Regulation of the European Parliament and of the Council Laying Down Harmonised Rules on Artificial Intelligence (Artificial Intelligence Act) and Amending Certain Union Legislative Acts (2021).
URL <https://eur-lex.europa.eu/legal-content/EN/TXT/?uri=CELEX:52021PC0206>
- [19] S. M. Lundberg, G. Erion, H. Chen, A. DeGrave, J. M. Prutkin, B. Nair, R. Katz, J. Himmelfarb, N. Bansal, S.-I. Lee, From local explanations to global understanding with explainable ai for trees, *Nature Machine Intelligence* 2 (1) (2020) 56–67. doi:10.1038/s42256-019-0138-9.
URL <https://doi.org/10.1038/s42256-019-0138-9>
- [20] M. T. Ribeiro, S. Singh, C. Guestrin, “Why should i trust you?”: Explaining the predictions of any classifier, in: *Proceedings of the 22nd ACM SIGKDD International Conference on Knowledge Discovery and Data Mining, KDD ’16*, Association for Computing Machinery, New York, NY, USA, 2016, p. 1135–1144. doi:10.1145/2939672.2939778.
URL <https://doi.org/10.1145/2939672.2939778>
- [21] C. Molnar, *Interpretable Machine Learning*, Lulu.com, 2020.
- [22] M. T. Ribeiro, S. Singh, C. Guestrin, Anchors: high-precision model-agnostic explanations, in: *Proceedings of the Thirty-Second AAAI Conference on Artificial Intelligence and Thirtieth Innovative Applications of Artificial Intelligence Conference and Eighth AAAI Symposium on Educational Advances in Artificial Intelligence, AAAI’18/IAAI’18/EAAI’18*, AAAI Press, New Orleans, Louisiana, USA, 2018, pp. 1527–1535.
- [23] R. Guidotti, A. Monreale, S. Ruggieri, D. Pedreschi, F. Turini, F. Giannotti, Local Rule-Based Explanations of Black Box Decision Systems, *arXiv:1805.10820 [cs]* (May 2018). doi:10.48550/arXiv.1805.10820.
URL <http://arxiv.org/abs/1805.10820>

- [24] P. Rasouli, I. C. Yu, Explan: Explaining black-box classifiers using adaptive neighborhood generation, in: 2020 International Joint Conference on Neural Networks (IJCNN), IEEE, 2020, pp. 1–9.
- [25] M. T. Ribeiro, S. Singh, C. Guestrin, Model-agnostic interpretability of machine learning (2016). [arXiv:1606.05386](https://arxiv.org/abs/1606.05386).
- [26] S. M. Lundberg, S.-I. Lee, A unified approach to interpreting model predictions, in: Proceedings of the 31st International Conference on Neural Information Processing Systems, NIPS’17, Curran Associates Inc., Red Hook, NY, USA, 2017, pp. 4768–4777.
- [27] S. M. Lundberg, G. G. Erion, S.-I. Lee, Consistent individualized feature attribution for tree ensembles (2019). [arXiv:1802.03888](https://arxiv.org/abs/1802.03888).
- [28] C. Rudin, Stop explaining black box machine learning models for high stakes decisions and use interpretable models instead, *Nature Machine Intelligence* 1 (5) (2019) 206–215. doi:10.1038/s42256-019-0048-x. URL <https://doi.org/10.1038/s42256-019-0048-x>
- [29] Y. Lou, R. Caruana, J. Gehrke, G. Hooker, Accurate intelligible models with pairwise interactions, in: Proceedings of the 19th ACM SIGKDD International Conference on Knowledge Discovery and Data Mining, KDD ’13, Association for Computing Machinery, New York, NY, USA, 2013, p. 623–631. doi:10.1145/2487575.2487579. URL <https://doi.org/10.1145/2487575.2487579>
- [30] A. Gosiewska, P. Biecek, ibreakdown: Uncertainty of model explanations for non-additive predictive models, *CoRR abs/1903.11420* (2019). [arXiv:1903.11420](https://arxiv.org/abs/1903.11420). URL <http://arxiv.org/abs/1903.11420>
- [31] I. Stepin, J. M. Alonso, A. Catala, M. Pereira-Fariña, A Survey of Contrastive and Counterfactual Explanation Generation Methods for Explainable Artificial Intelligence, *IEEE Access* 9 (2021) 11974–12001, conference Name: IEEE Access. doi:10.1109/ACCESS.2021.3051315.
- [32] R. K. Mothilal, A. Sharma, C. Tan, Explaining machine learning classifiers through diverse counterfactual explanations, in: Proceedings of the 2020 Conference on Fairness, Accountability, and Transparency, FAT* ’20, Association for Computing Machinery, New York, NY, USA, 2020, p. 607–617. doi:10.1145/3351095.3372850. URL <https://doi.org/10.1145/3351095.3372850>

- [33] B. Ustun, A. Spangher, Y. Liu, Actionable recourse in linear classification, in: Proceedings of the Conference on Fairness, Accountability, and Transparency, FAT* '19, Association for Computing Machinery, New York, NY, USA, 2019, p. 10–19. doi:10.1145/3287560.3287566. URL <https://doi.org/10.1145/3287560.3287566>
- [34] M. Pawelczyk, S. Bielawski, J. van den Heuvel, T. Richter, G. Kasneci, Carla: A python library to benchmark algorithmic recourse and counterfactual explanation algorithms (2021). arXiv:2108.00783.
- [35] E. Kaufmann, S. Kalyanakrishnan, Information complexity in bandit subset selection, in: Annual Conference Computational Learning Theory, 2013.
- [36] D. Macha, M. Kozielski, Łukasz Wróbel, M. Sikora, Rulexai—a package for rule-based explanations of machine learning model, SoftwareX 20 (2022) 101209. doi:<https://doi.org/10.1016/j.softx.2022.101209>. URL <https://www.sciencedirect.com/science/article/pii/S2352711022001273>
- [37] C. Aytekin, Neural networks are decision trees (2022). arXiv:2210.05189.
- [38] D. Collaris, J. J. van Wijk, ExplainExplore: Visual Exploration of Machine Learning Explanations, in: 2020 IEEE Pacific Visualization Symposium (PacificVis), 2020, pp. 26–35, iSSN: 2165-8773. doi:10.1109/PacificVis48177.2020.7090.
- [39] D. Collaris, J. J. van Wijk, Comparative evaluation of contribution-value plots for machine learning understanding, Journal of Visualization 25 (1) (2022) 47–57. doi:10.1007/s12650-021-00776-w. URL <https://doi.org/10.1007/s12650-021-00776-w>
- [40] L. Coroama, A. Groza, Evaluation metrics in explainable artificial intelligence (xai), in: T. Guarda, F. Portela, M. F. Augusto (Eds.), Advanced Research in Technologies, Information, Innovation and Sustainability, Springer Nature Switzerland, Cham, 2022, pp. 401–413.
- [41] S. Bobek, M. Kuk, J. Brzegowski, E. Brzychczy, G. J. Nalepa, KnAC: an approach for enhancing cluster analysis with background knowledge and explanations, Applied Intelligence (Nov. 2022). doi:10.1007/s10489-022-04310-9. URL <https://doi.org/10.1007/s10489-022-04310-9>

- [42] S. Bobek, M. Kuk, M. Szelażek, G. J. Nalepa, Enhancing cluster analysis with explainable ai and multidimensional cluster prototypes, *IEEE Access* 10 (2022) 101556–101574. doi:10.1109/ACCESS.2022.3208957.
- [43] J. Jakubowski, P. Stanisz, S. Bobek, G. J. Nalepa, Anomaly detection in asset degradation process using variational autoencoder and explanations, *Sensors* 22 (1) (2022). doi:10.3390/s22010291.
URL <https://www.mdpi.com/1424-8220/22/1/291>
- [44] A. Páez, The pragmatic turn in explainable artificial intelligence (XAI) 29 (3) 441–459. doi:10.1007/s11023-019-09502-w.
URL <https://doi.org/10.1007/s11023-019-09502-w>
- [45] R. R. Selvaraju, M. Cogswell, A. Das, R. Vedantam, D. Parikh, D. Batra, Grad-CAM: Visual Explanations from Deep Networks via Gradient-Based Localization, in: *2017 IEEE International Conference on Computer Vision (ICCV)*, 2017, pp. 618–626, iSSN: 2380-7504. doi:10.1109/ICCV.2017.74.
- [46] J. Suh, S. Ghorashi, G. Ramos, N.-C. Chen, S. Drucker, J. Verwey, P. Simard, AnchorViz: Facilitating Semantic Data Exploration and Concept Discovery for Interactive Machine Learning, *ACM Transactions on Interactive Intelligent Systems (TiS)* 10 (1) (Aug. 2019).
- [47] M. Ankerst, M. M. Breunig, H.-P. Kriegel, J. Sander, Optics: Ordering points to identify the clustering structure, *SIGMOD Rec.* 28 (2) (1999) 49–60. doi:10.1145/304181.304187.
URL <https://doi.org/10.1145/304181.304187>
- [48] H. Han, W.-Y. Wang, B.-H. Mao, Borderline-smote: A new over-sampling method in imbalanced data sets learning, in: D.-S. Huang, X.-P. Zhang, G.-B. Huang (Eds.), *Advances in Intelligent Computing*, Springer Berlin Heidelberg, Berlin, Heidelberg, 2005, pp. 878–887.
- [49] S. Bobek, G. J. Nalepa, Uncertainty handling in rule-based mobile context-aware systems, *Pervasive and Mobile Computing* 39 (2017) 159–179. doi:<https://doi.org/10.1016/j.pmcj.2016.09.004>.
URL <https://www.sciencedirect.com/science/article/pii/S1574119216302115>
- [50] S. Bobek, P. Misiak, Uncertain decision tree classifier for mobile context-aware computing, in: L. Rutkowski, R. Scherer, M. Korytkowski, W. Pedrycz, R. Tadeusiewicz, J. M. Zurada (Eds.), *Artificial Intelligence and Soft*

Computing - 17th International Conference, ICAISC 2018, Zakopane, Poland, June 3-7, 2018, Proceedings, Part II, Vol. 10842 of Lecture Notes in Computer Science, Springer, 2018, pp. 276–287. doi:10.1007/978-3-319-91262-2_25.
URL https://doi.org/10.1007/978-3-319-91262-2_25

- [51] J. Gama, Oblique linear tree, in: Proceedings of the Second International Symposium on Advances in Intelligent Data Analysis, Reasoning about Data, IDA '97, Springer-Verlag, Berlin, Heidelberg, 1997, p. 187–198.
- [52] T. Elomaa, T. Malinen, On lookahead heuristics in decision tree learning, in: N. Zhong, Z. W. Raś, S. Tsumoto, E. Suzuki (Eds.), Foundations of Intelligent Systems, Springer Berlin Heidelberg, Berlin, Heidelberg, 2003, pp. 445–453.
- [53] D. Alvarez-Melis, T. S. Jaakkola, On the robustness of interpretability methodsCite arXiv:1806.08049Comment: presented at 2018 ICML Workshop on Human Interpretability in Machine Learning (WHI 2018), Stockholm, Sweden (2018).
URL <http://arxiv.org/abs/1806.08049>